


 CrossMark
click for updates

 Cite this: *CrystEngComm*, 2014, 16, 7869

 Received 13th May 2014,
Accepted 3rd July 2014

DOI: 10.1039/c4ce00999a

www.rsc.org/crystengcomm

Shape-controlled synthesis of copper telluride micro/nanostructures *via* a simple electrochemical deposition route

 Yonghong Ni,^{*a} Huying Zhang,^a Junjun Xi,^a Xuemei Wang,^a Yongmei Zhang,^a Yanling Xiao,^a Xiang Ma^b and Jianming Hong^b

Shape-controllable synthesis of copper telluride micro/nanostructures has been successfully realized in air at room temperature by a simple galvanostatic electrodeposition route. By tuning experimental parameters such as the original Cu and Te sources, additives, deposition currents and media, copper telluride micro/nanostructures with various morphologies, including nanorod arrays, nanosphere-strewn copper telluride dendrites, copper telluride nanowires and star-like hexagonal copper telluride dendrites, were rapidly deposited in air at room temperature for 5 min. The final products were characterized by various means including X-ray diffraction, scanning electron microscopy, (high-resolution) transmission electron microscopy, and energy-dispersive spectrometry. The mechanisms of copper telluride production in various media are discussed.

1. Introduction

Over the past two decades, copper tellurides have been receiving considerable attention due to their potential applications in various devices such as solar cells, superionic conductors, photodetectors, photothermal conversion, electroconductive electrodes, microwave-shielding coatings, and optical data storage.^{1–8} Also, copper tellurides are important for foundational study owing to their large number of compositions including stoichiometric CuTe, Cu₄Te₃, Cu₇Te₅, Cu₇Te₄, Cu₂Te and nonstoichiometric Cu_{2–x}Te.⁹

Previous reports mainly focused on the thin-film materials and bulk materials of copper tellurides.^{4,7,10} In recent years, nanostructured copper tellurides, including nanoparticles, nanorods, nanowires and nanoribbons, have been successfully

synthesized by various methods. For example, Kumar and Singh prepared Cu₂Te nanoparticles on a large scale by employing an element-directed wet chemical route.¹¹ She *et al.* synthesized CuTe nanoribbons through a template-free electrochemical route.¹² Zhang *et al.* fabricated copper telluride nanowires/nanorods in different media *via* a modified hydrothermal method.⁷ Yang *et al.* designed a hydrothermal reduction route to successfully prepare a series of non-stoichiometric copper telluride nanocrystallites.¹³ Li *et al.* reported the successful synthesis of nanocrystalline Cu₇Te₄ *via* a sonochemical approach or a solvothermal route.¹⁴ Sheet- and ribbon-like Cu₇Te₄ nanostructures were also obtained through an amine-assisted solvothermal route.^{15–17} In 2011, our group also successfully prepared dendritic Cu₇Te₄ superstructures constructed from spherical nanoparticles in HNO₃ medium *via* a simple electrochemical deposition route, employing Cu(CH₃COO)₂ and Na₂TeO₃ as the reactants without the assistance of any additive.¹⁴ However, the shape-controlled synthesis of copper telluride through a simple electrodeposition technology has not been reported in the literature to date.

In this paper, we employed simple electrochemical deposition routes to successfully realize the shape-controlled synthesis of copper telluride micro/nanostructures. All deposition processes were carried out in galvanostatic mode in air at room temperature for 5 min. Copper telluride micro/nanostructures with various shapes, including nanorod arrays, nanosphere-strewn dendrites, nanowires, and star-like hexagonal dendrites, were obtained by adjusting experimental parameters such as the original Cu ion sources, additives, media, and deposition currents. Also, the mechanisms of copper telluride production in various systems are discussed.

2. Experimental section

All reagents and chemicals were analytically pure, purchased from Shanghai Chemical Company and used without further purification.

^a College of Chemistry and Materials Science, Key Laboratory of Functional Molecular Solids of Education Ministry, Anhui Laboratory of Molecule-Based Materials, Anhui Key Laboratory of Functional Molecular Solids, Anhui Normal University, 1 Beijing East Road, Wuhu, 241000, PR China. E-mail: niyh@mail.ahnu.edu.cn; Fax: +86 553 3869303

^b Centres of Modern Analyses, Nanjing University, 23 Hankou Road, Nanjing, 210093, PR China

2.1 Shape-controlled synthesis of copper telluride micro/nanostructures

In a typical experiment, a conventional three-electrode cell is used, employing a Pt wire as the counter electrode, a saturated Ag/AgCl electrode as the reference electrode, and a Cu plate (99.99%, $1.0 \times 1.0 \text{ cm}^2$) as the working electrode. To successfully obtain the products with various shapes, different original electrolytes were prepared (see Table 1). The electrodeposition experiments were conducted in galvanostatic mode in air at room temperature for 5 min. The volumes of all electrolytes were 30 mL.

2.2 Characterization

The X-ray diffraction (XRD) patterns of the electrodeposited products were recorded on a Shimadzu XRD-6000 X-ray diffractometer (Cu $K\alpha$ radiation, $\lambda = 0.154060 \text{ nm}$) at a scanning rate of 0.02 s^{-1} and a 2θ range of 10° to 80° . Field emission scanning electron microscopy (SEM) images and energy-dispersive spectra (EDS) of the final products were taken on a Hitachi S-4800 field emission scanning electron microscope at accelerating voltages of 5 and 15 kV, respectively. For EDS analyses, small amounts of products were removed from the Cu plate and fixed to a Ni substrate with double-sided adhesive tape to avoid interference of the Cu substrate. High-resolution transmission electron microscopy (HRTEM) images were recorded on a JEOL 2010 transmission electron microscope at an accelerating voltage of 200 kV. The content of Cu_7Te_4 in the final product was analyzed by inductively coupled plasma atomic emission spectroscopy (ICP-AES, Optima 5300DV-ICP, Perkin-Elmer).

3. Results and discussion

3.1 Shape-controlled synthesis and characterization of copper telluride micro/nanostructures

The XRD patterns of the products obtained under various experimental conditions (see Table 1) are displayed in Fig. 1. One can easily observe that samples 2, 3 and 4 exhibit similar diffraction patterns but sample 5 does not; the diffraction peak intensities gradually decreased from sample 2 to sample 4. According to the XRD pattern of sample 2, most of the

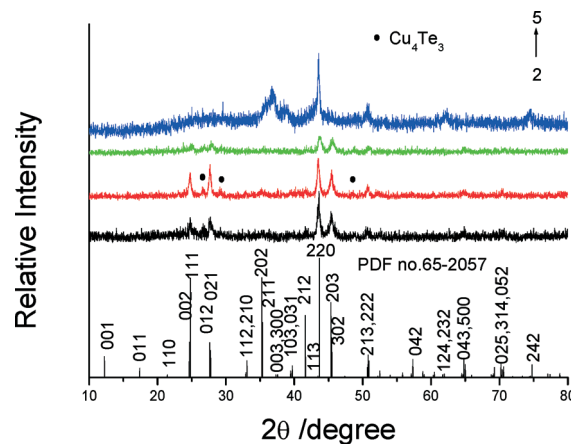


Fig. 1 XRD patterns of the products deposited by galvanostatic electrolysis in various systems for 5 min.

diffraction peaks can be indexed to the hexagonal Cu_7Te_4 form by comparison with the data for JCPDS card file no. 65-2057 (see Fig. 1 (bottom)). Three weak peaks centred at $\sim 26.5^\circ$, $\sim 29.2^\circ$ and $\sim 48.6^\circ$ can be attributed to the orthorhombic Cu_4Te_3 form (no. 42-1254), in good agreement with our previous work.¹⁸ ICP-AES analyses showed that all samples contained close contents of Cu_7Te_4 and Cu_4Te_3 . For example, the final product consisted of 67.4% Cu_7Te_4 and 32.6% Cu_4Te_3 in samples 2 and 3, 67.1% Cu_7Te_4 and 32.9% Cu_4Te_3 in sample 4, and 67.8% Cu_7Te_4 and 32.2% Cu_4Te_3 in sample 5. In the standard data, moreover, the (012) peak is far weaker than the (111) and (202) ones. However, the (202) peak could not be clearly detected in the XRD pattern of sample 2; simultaneously, the (012) peak exhibited a close intensity to the (111) one. The above phenomena imply the oriented growth of the final product. In sample 5, however, some diffraction peaks that were strong in samples 2–4 dramatically weakened or disappeared, *i.e.* the peaks located at 20° – 30° and the (203) one at 45.3° ; simultaneously, some weak peaks markedly increased, including the (003), (300), (103), (031), (124), (232) and (242) ones. The above facts likewise show the oriented growth of sample 5. To further analyze the compositions of samples 2–5, the EDS technique was employed. EDS analyses of the four samples are shown in Fig. 2. Distinctly, the four EDS spectra are similar except for their intensities.

Table 1 The original experimental parameters and the morphologies of the final products

Entry	Cu source	Te source	Surfactant	Medium	Complexant	pH	<i>I</i> /mA	Shape of the final product
1	CuAc_2^a 0.5 mmol	Na_2TeO_3 0.5 mmol	—	HNO_3 2 mL, 4.8 M	—	0.55	16	Dendrites built up of nanospheres ^c
2	Cu plate	Na_2TeO_3 1 mmol	SDBS ^b 0.1 mmol	HNO_3 3 mL, 3.6 M	—	0.56	16	Nanorod arrays
3	Cu plate	Na_2TeO_3 1 mmol	SDBS 0.1 mmol	HNO_3 3 mL, 3.6 M	Tartaric acid 1 mmol	0.50	16	Dendrites strewn with nanospheres
4	CuSO_4 2 mmol	TeO_2 0.5 mmol	—	KOH 5 mmol	—	11.65	4	Nanowires
5	CuSO_4 1 mmol	Na_2TeO_3 0.5 mmol	—	$\text{NH}_3 \cdot \text{H}_2\text{O}$ 25%, 12 mL	—	11.48	20	Star-like dendrites

^a CuAc_2 : $\text{Cu}(\text{CH}_3\text{COO})_2$. ^b SDBS: sodium dodecylbenzenesulfonate. ^c Ref. 18.

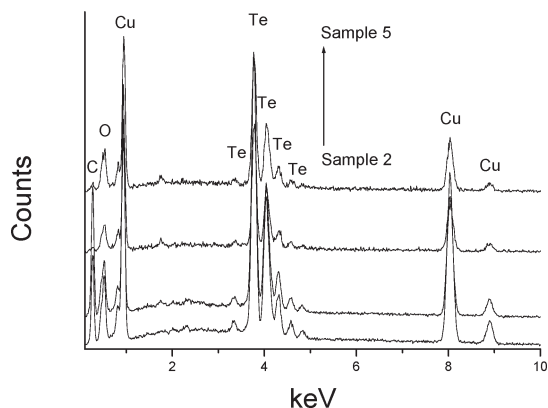


Fig. 2 EDS analyses of the products prepared by galvanostatic electrolysis from various systems for 5 min.

The strong Cu and Te peaks can be easily observed, confirming the formation of copper telluride. The C peaks in samples 2 and 3 are stronger than those in samples 4 and 5, which could be attributed to the residual organic additives in samples 2 and 3, such as SDBS and/or tartaric acid. Also, the EDS spectra of samples 4 and 5 can be fully superimposed on each other, indicating that they bear a similar chemical composition. Furthermore, the gradual decrease of the peak intensities in the XRD patterns from sample 2 to sample 4 could be related to the electrolytes. Based on the analyses of Table 1, one can find that strong diffraction peaks can be obtained in HNO_3 media (e.g. samples 2 and 3) while in KOH medium, the diffraction peaks weaken (sample 4). It is well known that $\text{Cu}(\text{OH})_2$ precipitates can be formed when Cu^{2+} and OH^- ions are mixed according to a 1:2 molar ratio, dramatically reducing the concentration of free Cu^{2+} ions in the electrolyte. In sample 4, Cu^{2+} ions, TeO_2 and KOH completely reacted to form $\text{Cu}(\text{OH})_2$ and K_2TeO_3 . Thus, the free Cu^{2+} ion concentration was dramatically reduced. In sample 5, excess ammonia was used. Thus, $[\text{Cu}(\text{NH}_3)_4]^{2+}$ complex ions were obtained, which also decreased the concentration of free Cu^{2+} ions. However, different deposition currents were employed in various systems. Therefore, different systems have different deposition, nucleation and growth rates. As a result, the final products deposited in different systems have different crystallinities.

The morphologies of the products were observed by SEM and TEM. Fig. 3–6 show the SEM and TEM images of samples 2–5, respectively. Obviously, the morphologies of all products are different. Sample 2 presents an array architecture built up of nanorods (see Fig. 3a). These nanorods are assembled from nearly spherical nanoparticles with diameters from ~20 nm to ~80 nm; the lengths of nanorods are ~1 μm . Although the orderly nanorod arrays have been broken by ultrasound during the TEM sample preparation, some rod-like structures built up of nanoparticles can still be found (see Fig. 3b). The sizes of most nanoparticles range from 20 to 40 nm, which are lower than those observed by SEM. This implies that the larger, nearly spherical nanoparticles shown in Fig. 3a comprise smaller nanoparticles.

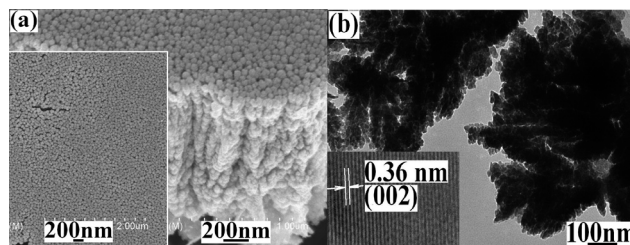


Fig. 3 Electron micrographs of the product prepared from the system containing 1.0 mmol of Na_2TeO_3 , 3 mL of 3.6 M HNO_3 , 0.1 mmol of SDBS at a deposition current of 16 mA for 5 min: (a) a lateral SEM image (the inset is a planform) and (b) a typical TEM image. The inset shown in (b) is an HRTEM image.

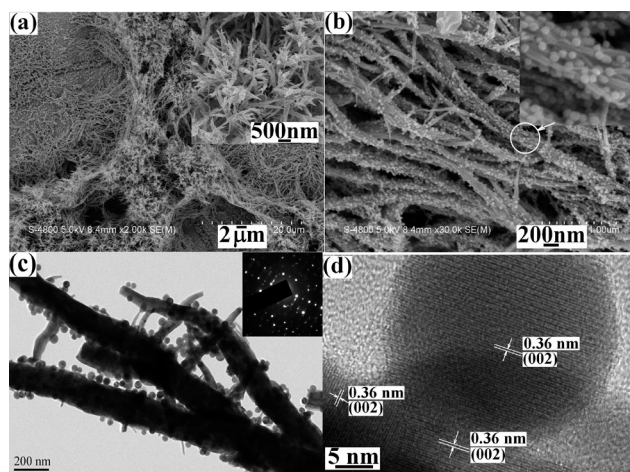


Fig. 4 Electron micrographs of the product prepared from the system containing 1.0 mmol of Na_2TeO_3 , 3 mL of 3.6 M HNO_3 , 0.1 mmol of SDBS and 1 mmol of tartaric acid at a deposition current of 16 mA for 5 min: (a) a representative low-magnification SEM image (the inset is a high-resolution SEM image of the top of dendrites), (b) a high-magnification SEM image of the stems, (c) a typical TEM image (the inset is a SAED pattern) and (d) an HRTEM image of the stem with a spherical nanoparticle.

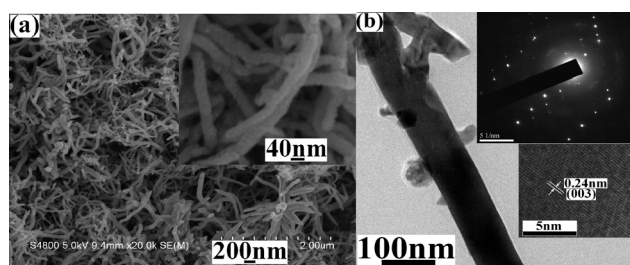


Fig. 5 Electron micrographs of the product prepared from the system containing 2.0 mmol of CuSO_4 , 0.5 mmol of TeO_2 and 5 mmol of KOH at a deposition current of 4 mA for 5 min: (a) a representative low-magnification SEM image (the inset is a high-resolution SEM image) and (b) a TEM image of nanowires (upper inset: an ED pattern; lower inset: an HRTEM image).

Sample 3 is composed of abundant undergrowth-like structures (see Fig. 4a and its inset). High-magnification SEM images show that many spherical nanoparticles with a diameter of ~30 nm are strewn on the stems (Fig. 4b) and

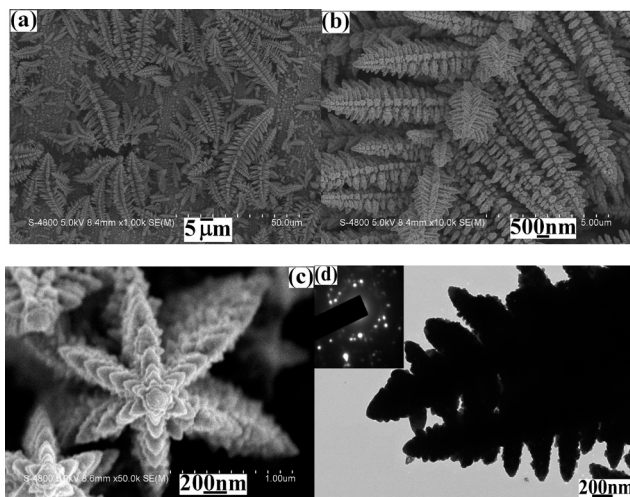


Fig. 6 Electron micrographs of the product prepared from the system containing 1.0 mmol of CuSO_4 , 0.5 mmol of Na_2TeO_3 and 12 mL of 25% $\text{NH}_3\cdot\text{H}_2\text{O}$ at a deposition current of 20 mA for 5 min: (a) a representative low-magnification SEM image, (b) a high-resolution SEM image, (c) a planform of the top of dendrites and (d) a TEM image (upper left inset: an ED pattern).

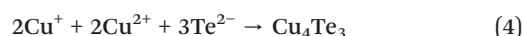
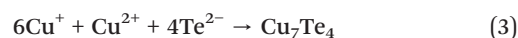
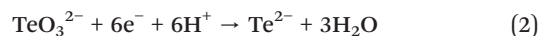
that the thick stems are made up of many thin nanowires (see the inset in Fig. 4b). The above results are confirmed by TEM observations (see Fig. 4c). Moreover, the HRTEM images depicted in the insets of Fig. 3b and 4d reveal good crystallinities of samples 2 and 3, respectively. The distances between the neighbouring planes were measured to be ~ 0.36 nm, which corresponds to the lattice spacing of 0.361 nm of the (002) plane of Cu_7Te_4 . According to Table 1, samples 2 and 3 were prepared under the same deposition conditions before and after the introduction of 1 mmol of tartaric acid, respectively. Therefore, they should have similar growth environments. It is well known that tartaric acid has strong coordination ability to Cu^{2+} ions. It is possible that copper telluride nuclei were surrounded by tartaric acid molecules, which limited the growth direction of copper telluride. As a result, the shape of copper telluride was converted from nanorod arrays to nanoparticle-strewn undergrowth-like microstructures.

Different from samples 2 and 3, samples 4 and 5 were deposited in basic systems. Their growth environments should be different from those in the acid ones. As shown in Fig. 5a, sample 4 was composed of a large number of wrapped nanowires with diameters ranging from 40 to 60 nm. However, these nanowires were not smooth. Some small nanoparticles and short nanorods grew on their surfaces (see Fig. 5b). The ED pattern and the HRTEM image confirmed the good crystallinity of the final product (see the insets in Fig. 5b). Here, the distance between neighbouring stripes of sample 4 is ~ 0.24 nm, which is very close to the lattice spacing of the (003) plane of Cu_7Te_4 . Sample 5 presented dendritic hierarchical microstructures (Fig. 6a and d). Each dendrite comprised several subbranches, and each subbranch was made up of smaller subbranches (Fig. 6b). All dendrites and subbranches present six-petal structures (see Fig. 6c). However, the SAED

pattern shown in the inset of Fig. 6d indicated the polycrystalline nature of the product. Distinctly, sample 4 had a different growth environment from sample 5 although both were deposited in basic systems.

3.2 Possible formation process

Based on the above results and Table 1, one can easily conclude that copper telluride can be deposited in various systems and that its morphology can be tuned by varying experimental parameters including electrodeposition media, surfactants and complexants, and deposition current. However, the formation mechanisms of copper telluride should be different in various systems. According to our previous report,¹⁸ in the acidic system where sample 1 was deposited, the formation of copper telluride underwent the following reactions:



Samples 2 and 3 were also deposited in HNO_3 media. Here, the Cu plate was used as the Cu source instead of Cu^{2+} ions and simultaneously additives were introduced. However, Cu can be oxidized to Cu^{2+} ions owing to the oxidation of HNO_3 . Thus, samples 2 and 3 were also formed according to the above reactions. The generated copper telluride gradually nucleated and grew to form nanospheres. With the assistance of additives, finally, nanospheres assembled into nanorod arrays (sample 2) or further grew into dendrites strewn with nanospheres (sample 3).

In basic systems, however, Cu^{2+} ions can react with OH^- and NH_3 to form $\text{Cu}(\text{OH})_2$ and $[\text{Cu}(\text{NH}_3)_4]^{2+}$ ions, respectively. In the current work, free Cu^{2+} ions were converted into $\text{Cu}(\text{OH})_2$ in the KOH system or into $[\text{Cu}(\text{NH}_3)_4]^{2+}$ complex ions in the aqueous ammonia system, resulting in the decrease of the Cu^{2+} ion concentrations in these systems. Due to the reaction between TeO_2 and KOH, the Te source was TeO_3^{2-} ions in both systems. Here, different from acidic systems, Te^{2-} ions could be generated in alkali systems according to eqn (5):



Simultaneously, Cu^+ could still be produced according to eqn (1) despite the low Cu^{2+} ion concentrations in the systems. Finally, copper telluride was formed according to eqn (3) and (4). Since the produced nanocrystals had different growth environments in KOH and NH_3 systems, the final products presented different shapes and crystallinity.

3.3 Influencing factors

As mentioned in the previous text, copper telluride micro/nanostructures with various shapes could be prepared by

varying experimental parameters. In fact, the formation of copper telluride with a certain shape is likewise affected by various parameters. Here, we selected the preparation of nanorod arrays as a case to investigate the influence of experimental parameters on the morphology of the final product.

During the synthesis of nanorod arrays, when the Cu and Te sources did not change, the main parameters included the type and amount of surfactant, the type of acid and the amount of nitric acid, the deposition current and the time. Among these, the surfactant and nitric acid are two important factors.

3.3.1 The influence of the surfactant. When no surfactant was used, the product consisted of abundant loose irregular nanoparticles and some feather-like flakes under the same experimental conditions (Fig. 7a). After 0.05 mmol of SDBS was introduced into the system, the morphology of the product markedly changed and thicket-like superstructures with long leaves on the top were obtained (Fig. 7b). When 0.1 mmol of SDBS was added, nanorod arrays assembled from a large number of near-spherical nanoparticles were obtained (Fig. 3). Upon further increasing the amount of SDBS, the nanorod arrays were always deposited. Fig. 7c and d show the representative SEM images of the products obtained in the presence of 0.2 mmol and 0.5 mmol of SDBS, respectively. The above experiments indicate that high SDBS concentration results in the formation of nanorod arrays. Furthermore, when SDBS was replaced by other surfactants with the same amount, such as polyvinylpyrrolidone (PVP) and cetyltrimethylammonium bromide (CTAB), SEM observations showed that flower-like and feather-like superstructures were obtained under the same experimental conditions, respectively (see Fig. 8). No nanorod arrays were formed in the presence of the above two surfactants. Generally, HTeO_2^+ ions are considered to be the main existence fashion of original tellurium source in diluted HNO_3 solution.¹⁹ When SDBS, an anion surfactant, exists in the system, it could be attracted to HTeO_2^+ ions due

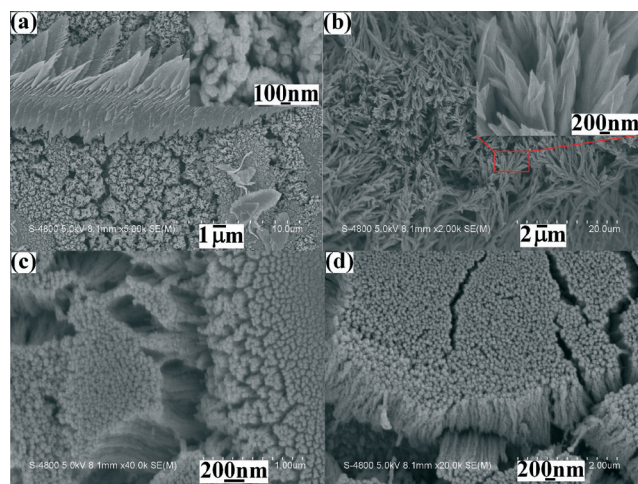


Fig. 7 SEM images of the final product obtained under the same conditions with different amounts of SDBS in the system: (a) 0.0, (b) 0.05 mmol, (c) 0.2 mmol and (d) 0.5 mmol.

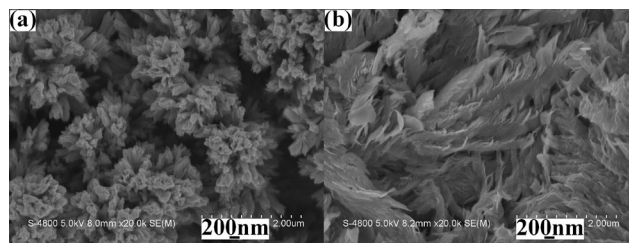


Fig. 8 SEM images of the products obtained under the same conditions in the presence of different surfactants: (a) PVP and (b) CTAB.

to their opposite charges. This would strongly affect the morphology of the final product, which has been proven by SEM observations (Fig. 7). Based on the results of SEM observations, SDBS could act as both a structure-directing agent and a surfactant. At low SDBS amounts, *e.g.* 0.05 mmol, it mainly acted as a structure-directing agent. Thus, thicket-like superstructures with long leaves on the top were obtained (Fig. 7b). With the increase in the amount of SDBS in the system, however, the surfactant function could not be ignored. When the above two roles cooperated, nanorod arrays assembled from a large number of near-spherical nanoparticles were obtained. In PVP molecules, some atoms such as N and O have stronger coordination abilities. It is possible that copper telluride nuclei were surrounded by PVP due to certain weak interactions between N and Cu. As a result, flower-like superstructures were deposited (Fig. 8a). However, CTAB is a cationic surfactant, which would be far away from HTeO_2^+ ions in the present system owing to the repulsion between like charges. Thus, the product was mainly composed of feather-like flakes (Fig. 8b).

3.3.2 The influence of HNO_3 . Furthermore, HNO_3 could also strongly affect the formation of nanorod arrays. When HNO_3 was not introduced into the system, no product was deposited under the present deposition conditions. After 2 mL of 3.6 M HNO_3 was added under the same deposition conditions long vine-shaped products were obtained (Fig. 9a, the inset is a planform). When 3 mL of 3.6 M HNO_3 was employed, nanorod arrays were deposited (Fig. 3). Upon further increasing the volume of 3.6 M HNO_3 to 5 mL and 7 mL, nanorod arrays were still formed (Fig. 9b and c). After addition of more than 7 mL of 3.6 M HNO_3 , however, the nanorod arrays changed, becoming loose and irregular. Interestingly, when HNO_3 was replaced by H_2SO_4 or HClO_4 with the same H^+ ion concentration, the deposition reaction did not occur, confirming that HNO_3 is indispensable in the formation of nanorod arrays. It is well known that HNO_3 is an oxidative acid. It can oxidize copper atoms on the surface of the Cu plate used as the Cu ion source. However, diluted H_2SO_4 or HClO_4 is non-oxidative, thus copper atoms on the surface of the Cu plate cannot be activated by them. Therefore, different results are obtained.

3.3.3 The influence of the deposition time. Fig. 10 shows SEM images of the products deposited at various durations. At the initial stage of deposition (*e.g.* 10 s), some sheet-like

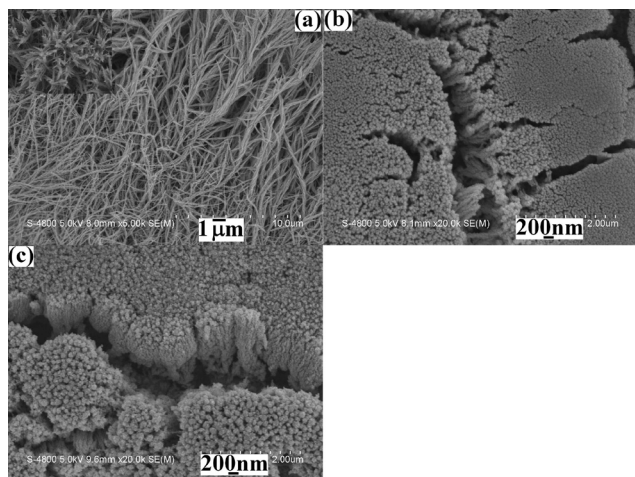


Fig. 9 SEM images of the products prepared under the same deposition conditions from the system containing various volumes of 3.6 M HNO₃: (a) 2 mL, (b) 5 mL and (c) 7 mL.

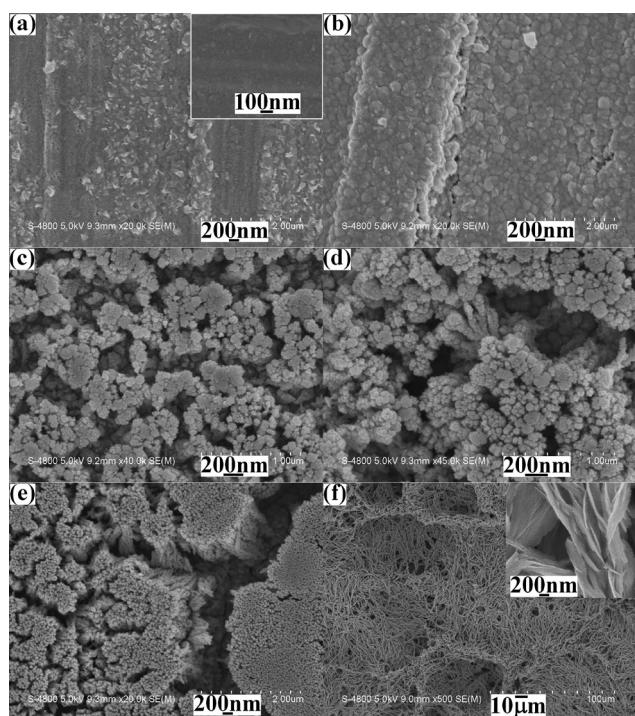


Fig. 10 SEM images of the products prepared under the same experimental conditions at various deposition times: (a) 10 s, (b) 30 s, (c) 60 s, (d) 90 s, (e) 3 min and (f) 10 min.

particles were deposited on the Cu substrate (see Fig. 10a, the inset is a SEM image of the Cu substrate.). After 30 s of deposition, a film consisting of abundant nanoparticles was obtained (Fig. 10b). Upon further prolonging the deposition duration to 60 and 90 s, immature arrays started to appear (Fig. 10c and d). After 3 min, ordered arrays on the Cu substrate were formed (Fig. 10e). When the deposition time was prolonged to 5 min, compact and ordered Cu₇Te₄ nanorod

arrays were obtained with relatively uniform sizes (see Fig. 3). If longer deposition durations were employed, *e.g.* 10 min, the final product comprised a large number of undergrowths of ~80 μm in length (Fig. 10f). The tops of the undergrowths exhibited leaf-like structures which were constructed from a large number of nanosheets (see the inset in Fig. 10f). The above experimental facts clearly demonstrate that the formation of nanorod arrays derives from the vertically oriented assembly/growth of the nanoparticle film deposited on the Cu substrate. As mentioned in the previous text, HTeO₂⁺ ions could be formed due to the reaction between Na₂TeO₃ and HNO₃. At the deposition current of 16 mA, copper telluride was rapidly generated, nucleated and grew into particle films (Fig. 10a and b). With the assistance of SDBS, freshly produced copper telluride nanoparticles ceaselessly grew on the above particle film. Thus, nanorod arrays consisting of abundant nanoparticles were finally obtained.

Furthermore, experiments revealed that low or high deposition currents did not lead to the formation of nanorod arrays and that 16 mA is the optimum current.

4. Conclusions

In summary, shape-controllable syntheses of copper telluride micro/nanostructures have been successfully realized *via* a simple electrodeposition route in air at room temperature by employing different electrodeposition media, additives and deposition currents. All copper telluride micro/nanostructures were obtained within 5 min. ICP-AES analyses showed that all samples have similar contents of Cu₇Te₄ and Cu₄Te₃. For samples 2 to 5, the content of Cu₇Te₄ was 67.4%, 67.4%, 67.1% and 67.8%, respectively. Copper telluride dendrites constructed from spherical nanoparticles were prepared at a deposition current of 16 mA using CuSO₄, Na₂TeO₃ and diluted HNO₃ as the original reactants without the assistance of any additives.¹⁸ Under the same deposition current, copper telluride nanorod arrays were deposited by employing a Cu plate, Na₂TeO₃ and diluted HNO₃ as the original reactants in the presence of sodium dodecylbenzenesulfonate while nanosphere-strewn copper telluride dendrites were synthesized after a suitable amount of tartaric acid was introduced to the above system. However, copper telluride nanowires were prepared at a deposition current of 4 mA by utilizing CuSO₄, TeO₂ and KOH as raw materials while star-like copper telluride dendrites were obtained at a deposition current of 20 mA, with CuSO₄, Na₂TeO₃ and NH₃·H₂O as the electrolytes. Furthermore, experiments found that HNO₃ and SDBS are two indispensable factors for the formation of copper telluride nanorod arrays.

Acknowledgements

The authors thank the National Natural Science Foundation of China (21171005) and the Key Foundation of Chinese Ministry of Education (210098) for fund support.

References

- 1 T. Nishio, M. Takahashi, S. Wada, T. Miyauchi, K. Wakita, H. Goto, S. Sato and O. Sakurada, *Electr. Eng. Jpn.*, 2008, **164**, 12.
- 2 C. Nascu, I. Pop, V. Ionscu, E. Indra and I. Bratu, *Mater. Lett.*, 1997, **32**, 73.
- 3 X. Wang, J. Wang, M. Zhou, H. Zhu, H. Wang, X. Cui, X. Xiao and Q. Li, *J. Phys. Chem. C*, 2009, **113**, 16951.
- 4 H. M. Pathan, C. D. Lokhande, D. P. Amalnerkar and T. Seth, *Appl. Surf. Sci.*, 2003, **218**, 290.
- 5 F. Caballero-Briones, A. Palacios-Padrós, J. L. Peña and F. Sanz, *Electrochem. Commun.*, 2008, **10**, 1684.
- 6 M. A. Korzhuev, *Phys. Solid State*, 1998, **40**, 217.
- 7 L. Z. Zhang, Z. H. Ai, F. L. Jia, L. Liu, X. L. Hu and J. C. Yu, *Chem. – Eur. J.*, 2006, **12**, 4185.
- 8 F. Hanus and L. D. Laude, *Proc. SPIE*, 1990, **1279**, 196.
- 9 A. S. Pashinkin and L. M. Pavlova, *Inorg. Mater.*, 2005, **4**, 939.
- 10 K. Neyvasagam, N. Soundararajan, Ajaysoni, G. S. Okram and V. Ganesan, *Phys. Status Solidi B*, 2008, **245**, 77.
- 11 P. Kumar and K. Singh, *Cryst. Growth Des.*, 2009, **9**, 3089.
- 12 G. W. She, X. H. Zhang, W. S. Shi, Y. Cai, N. Wang, P. Liu and D. M. Chen, *Cryst. Growth Des.*, 2008, **8**, 1789.
- 13 J. Yang, S. H. Yu, Z. H. Han, Y. T. Qian and Y. H. Zhang, *J. Solid State Chem.*, 2009, **146**, 387.
- 14 (a) B. Li, Y. Xie, J. X. Huang, Y. Liu and Y. T. Qian, *Chem. Mater.*, 2000, **12**, 2614; (b) B. Li, Y. Xie, J. X. Huang, H. L. Su and Y. T. Qian, *J. Solid State Chem.*, 1999, **146**, 47.
- 15 Q. Wang, G. Chen, D. H. Chen and R. C. Jin, *CrystEngComm*, 2012, **14**, 6962.
- 16 Q. Wang, G. Chen, X. R. Shi, R. C. Jin, L. Wang and D. H. Chen, *Powder Technol.*, 2011, **207**, 192.
- 17 X. R. Shi, Q. Wang, L. Y. Lu, Y. Li, X. Yu and G. Chen, *J. Inorg. Mater.*, 2012, **27**, 433.
- 18 Y. M. Zhang, Y. H. Ni, X. M. Wang, J. Xia and J. M. Hong, *Cryst. Growth Des.*, 2011, **11**, 4368.
- 19 F. Xiao, B. Yoo, M. A. Ryan, K. H. Lee and N. V. Myung, *Electrochim. Acta*, 2006, **52**, 1101.